Interactive Design and Analysis Program for Switched Reluctance Motor using an Analytical Method

[1] Pan Seok Shin, [2] Pedro J. Otaduy, John McKeever, and Don Adams

[1] Department of Electrical Engineering, Hongik University, Chochiwon, ChungNam, Korea 339-701
[2] PEEMRC, Oak Ridge National Laboratory, Knoxville, TN 37932, USA

Abstract-- This paper describes an interactive design and analysis tool for switched reluctance motors consisting of a module to estimate basic averaged performance parameters and a CAD program. The methodologies used follow conventional approaches. The CAD module calculates flux linkages, inductances and torque numerically as a function of rotor position and stator voltage. Dynamic performance of the motor can be performed with voltage and current control. Two SRMs designed for prospective use in electric vehicles were simulated. The calculated results are compared with the manufacturer specified values and with measured values.

I. Introduction

Switched Reluctance Motors (SRM), have advantages such as rotor simplicity, high-speed operation, ease of repair, high degree of independence between phases, wide speed range at constant power, short end-turn, and low inertia. Disadvantages include rotor position sensing complexity, small air gap, small shaft diameter, torque ripple, high temperature, high kVA requirement, and acoustic noise. In this paper, we describe physics-based models that can be used to evaluate traction drive systems for hybrid electric vehicles. Two SRMs acquired from vendors interested in their use in electric vehicles, were used to verify the software program.

The SRM design and simulation program is implemented with an interactive front end using *LabVIEW*. The program follows a five-step approach. Steps 1 through 3 define the motor. Step 1 requires input of primary performance, electrical and mechanical specifications, such as, mean torque, rotor speed, supply voltage, number of phases, number of stator poles and number of rotor poles. Step 2 includes envelope dimensions of the rotor and stator. Step 3 includes internal dimensions such as pole and slot depths and widths. In Step 4 the motor is sized and scaled drawings of the stator and rotor are produced. In addition, estimates of inductance, resistance, currents, power output, efficiency and motor weight are computed. While inside steps 1 through 4 any change of input values triggers automatic redrawing and recalculation of all performance parameters. In step 5, the CAD module performs a more detailed analysis based on rotor position dependent waveforms. The CAD's simulation algorithm performs a single pole flux-linkage analysis for the source voltage, current control, and firing and turn-off angles specified by the user. Based on symmetries the phase current, back emf, inductance, average torque and output power thus computed are cloned to generate the waveforms for the rest of poles and phases.

Fig. 1 shows the shape of the 12 kW SRM described in this study. The motor has 6-rotor poles and 8 stator slots. The steel core is M19 with relative permeability of 4500 and saturation flux density of 1.95 Tesla. The stator windings are connected in series and the power supply is a 4-phase inverter with 220 Volt DC source.

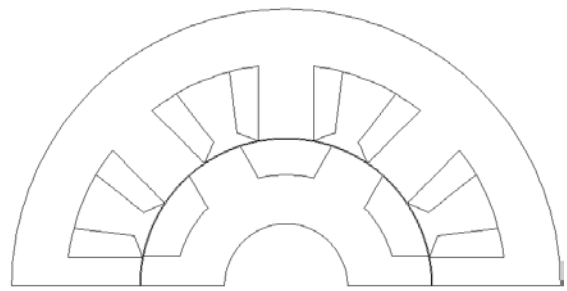

Fig.1
Schematic of the 8/6-pole, 12 kW SRM in unaligned position.

II. Analytical Formulation

Computation of the performance of an SRM requires the calculation of inductances and flux linkages as a function of rotor position and magnitude of the stator current.

A. Calculation of inductance and flux linkages in the unaligned region

When the active stator pole does not overlap a rotor tooth, i.e., it is between the tips of two adjacent rotor teeth – the so-called unaligned region of rotor position - the large air path between the stator tooth and rotor core keeps stator currents below magnetic saturation levels. The calculation of the unaligned inductance follows the approach by Radun (ref 5.)

$$L_u(\theta_u) = \frac{n_{ser}}{n_{par}} 4\mu_0 N_{tp}^{\ 2} L_{stk} l_{rsw} \sum_{nodd} \frac{\sin\left[\frac{n\pi d_1(\theta_u)}{l_{rsw}}\right]/l_1(\theta_u) + \sin\left[\frac{n\pi d_2(\theta_u)}{l_{rsw}}\right]/l_2(\theta_u)}{(n\pi)^2 \tanh\left[\frac{n\pi d_r}{l_{rsw}}\right]} \quad (1)$$

[1] mail to: psshin@wow.hongik.ac.kr
[2] mailto: otaduyp@ornl.gov, mckeeverjw@ornl.gov, adamsdj@ornl.gov

where, N_{tp} is the number of turns per pole, l_{rsw} is the rotor slot width, L_{stk} is motor stack length, $l_1(\theta_u)$ and $l_2(\theta_u)$ are the distances from the left and right tips of the stator pole to their closest rotor pole tip, n_{par} and n_{ser} are the number of pole windings connected in parallel and *in* series, respectively. The unaligned inductance in Eq. (1) results from integration of Faraday's law over the surface between the tips of adjacent rotor poles. The magnetic field is computed by means of the series expansion solution of Laplace's equation in a 2-D simplified rectangular geometry based on Fig. 1. This equation (Eq. 1) does not account for the contribution of the end-turns. The end-turn component is negligible and can be calculated conventionally [ref. 2]. The unaligned inductance is minimum when $l_1 = l_2$ i.e., when the stator tooth is centered in the gap between adjacent rotor teeth. From Eq 1, the flux linkage in the unaligned region for a phase current I_{ph}, is given by

$$\lambda(\theta_u, I_{ph}) = L_u(\theta_u) I_{ph} \tag{2}$$

B. Calculation of inductance and flux linkages in the Aligned region

As the rotor and stator poles start to overlap the reluctance decreases rapidly and dramatically so that currents high enough to cause magnetic saturation in the iron can occur for the original driving voltage. As the air gap between the stator and rotor teeth is reduced the dependence of iron's permeability on current dominates the electromagnetics of SRM systems. Calculation of the aligned inductance involves the partition of magnetic flux in two components: a main flux, λ_m, and a fringing flux, λ_f. A common assumption is to neglect the magnetomotive losses in the stator and rotor yokes and to assume that the flux density, B_m, in the stator tooth is the same as in the air gap between the stator and rotor teeth.

Using Ampere's Law, the current at which saturation occurs can be calculated.

$$I_{sat} = \frac{g\, B_{sat}}{\mu_0\, N_{tp}} \tag{3}$$

where I_{sat} is the saturating current, g is the air gap length, B_{sat} is the iron's saturation flux density, and μ_0 is the permeability of air. Then the flux linked by a phase in the presence of saturation can be approximated as

$$\lambda_\phi = \alpha\, k_{stf}\; L_{stk}\; t_{spw}\; B_{sat}\, 2N_{tp} \tag{4}$$

where α is the fraction of rotor and stator pole overlap, t_{spw} is the rotor pole pitch, and k_{stf} is the lamination stacking factor. To compute the flux linkage curves of the SRM analytically, Ampere's law is first applied to the closed contour lines.

$$H_{fe}\; 2\, l_p + H_g 2\, g = 2\, N_{tp}\; I_p \tag{5}$$

where H_{fe} is a field intensity in the core and in the rotor, l_p is a sum of the stator and pole lengths, and I_p is the pole current. The pole current, I_p, is equal to the phase current, I_{ph}, when the pole windings are in series, and it is equal to the phase current divided by the number of poles per phase when the pole windings are in parallel. The flux density in the air gap of the main flux contour is

$$B_m = \mu_0\; H_g\,. \tag{6}$$

while in the teeth and yoke iron along the main flux contour,

$$B_m(H_{fe}) = \tilde{\mu} H_{fe} \,/(1 + \frac{\tilde{\mu} H_{fe}}{B_{sat}}) + \mu_0\; H_{fe} \tag{7}$$

Eq. 7 describes the (B,H) dependence of the material with two parameters, $\tilde{\mu}$ and B_{sat}. In it, $\tilde{\mu}$ is the permeability associated with the magnetization $M = \mu_0\; \chi_m\, H$, where $\chi_m = \mu_r - 1$ is the magnetic susceptibility. By replacing $\tilde{\mu}$ by μ for convenience a small difference in B for small H occurs; $\mu_0(\mu_r + 1)H$ instead $\mu_0\mu_r H$. Assuming that the two flux densities are equal, equations (5), (6) and (7) turn into a quadratic equation for B_m whose solution is

$$B_m(I_{ph}) = \frac{\mu_0\, N_{tp}}{2\left(1 + \frac{g}{l_p}\right) g}\left(1 + \frac{2g}{l_p}\right)\frac{I_{ph}}{n_{par}} + \frac{l_{m1} B_{sat}}{\mu\, N_{tp}} - \sqrt{\left(\frac{l_{m1}\, B_{sat}}{\mu\, N_{tp}}\right)^2 + \frac{2 l_{m2}\, B_{sat}}{\mu\, N_{tp}}\frac{I_{ph}}{n_{par}} + \left(\frac{I_{ph}}{n_{par}}\right)^2}\,] \tag{8}$$

where $l_{m1} = l_p + (\mu_r + 1)g$, $l_{m2} = l_p - (\mu_r - 1)g$. This flux density in turn integrated over the cross-sectional area of the pole overlap yields the contribution of the main flux path to the flux linked by the phase coils. The main flux contribution to the total flux linked by a phase is then found to be

$$\lambda_m(\theta_a, I_{ph}) = n_{ser}\; N_{tp}\; L_{stk}\; k_{stf}\; R_g\; \theta_a\; B_m \tag{9}$$

where θ_a is the angle of overlap in the aligned region and R_g is the outer radius of the rotor.

The fringing flux from the stator pole enters the rotor through the yoke and the nearby poles. It is calculated using the following equation.

$$\lambda_f(\theta_a, I_{ph}) = n_{ser}\; N_{tp}\; L_{stk}\; k_{stf}\left(\frac{t_{spw} - R_g\theta_a}{g_f}\right) B_m \tag{10}$$

where, $g_f(\theta_a) = g + g_0\left(1 - R_g\, \theta_a / t_{spw}\right)$, and μ_r is the relative permeability of the iron. In the program g_0 is chosen to obtain the value of inductance, L_{po}, that is required at the rotor position where the rotor and stator poles just start to overlap, i.e., at $\theta_a = 0$. The total flux linked by the stator coils is the sum of the main flux, λ_m, and the fringing flux, λ_f. Fig. 2 shows the flux linkage curves computed for the 8/6 pole, 12kW SRM. A relative permeability μ_r of 2500, saturation flux density B_{sat} of 2.0 Tesla and stacking factor of 0.9 were used.

The calculation of flux linkages in the transition region between the unaligned and aligned regions is a challenge since

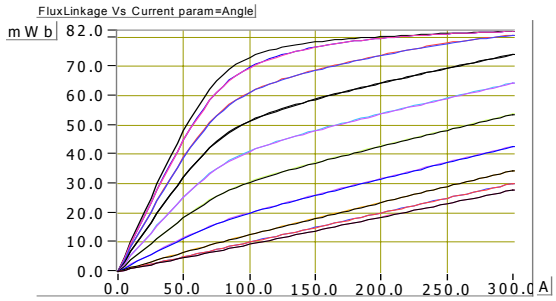

Fig. 2
Flux linkage vs.current curves as function of rotor position for the 8/6 pole, 12 kW SRM.

discontinuities at the transition point produce localized non-physical results. In our implementation two different smoothing algorithms are used to prevent abrupt discontinuities in the slope of flux links with rotor position. Fig. 3 shows the corresponding inductances calculated by

$$L(\theta, I_{ph}) = \left[\Delta\lambda / \Delta I_{ph} \right]_{\theta=const} . \qquad (11)$$

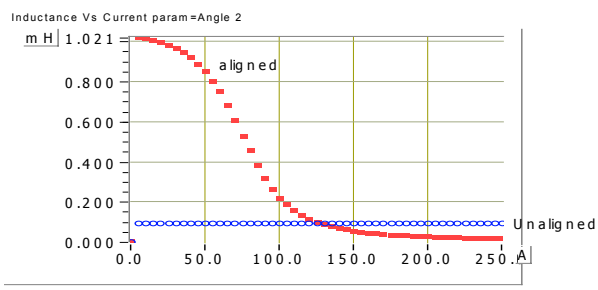

Fig. 3
Fully aligned and unaligned inductances of the 8/6 pole, 12 kW SRM

The unaligned inductance has a minimum value of 0.11 mH and slightly increases as the rotor approaches the stator pole tip. When the poles overlap, the inductance increases almost linearly to its maximum aligned value of 1.02 mH.

C. *Dynamic analysis of SRM performance*

The SRM's terminal voltage is governed by

$$V_s = R_{ph} I_{ph} + \frac{\partial \lambda_\phi}{\partial I_{ph}} \frac{dI_{ph}}{dt} + \frac{\partial \lambda_\phi}{\partial \theta_m} \omega_m \qquad (12)$$

where R_{ph} is the phase resistance of the SRM's stator windings and ω_m is the angular speed of the rotor. The terms in Eq.12 account for the ohmic, inductive and back EMF voltage components respectively. The interdependence of current and flux linkage requires iterative approaches to the solution of this equation.

Flux linkage increases almost linearly up to a peak value and, in order to prevent a braking torque, must be reduced to zero by the time the stator and rotor poles begin to separate. Consequently the polarity of the supplied voltage, V_s, must be reversed in advance of the point of separation.

The torque produced by the SRM is calculated from the changes in coenergy as follows

$$T_{static}(\theta, I_{ph}) = \left[\frac{\partial W_{co}(\theta, I_{ph})}{\partial \theta} \right]_{I_{ph}=const} \qquad (13)$$

where W_{co} is the co-energy calculated using the rotor position dependent flux linkage versus current curves. Fig. 4 shows a schematic diagram for the change in co-energy associated to a small change in rotor position. The area OAB represents the torque produced in the process.

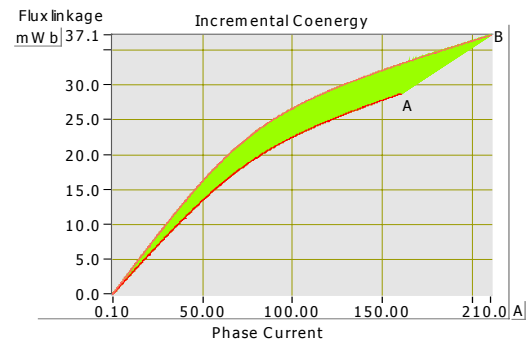

Fig. 4
Schematic diagram for the change in co-energy between two rotor positions.

Fig. 5 shows the flux linkage-current curves and an energy conversion loop of the 8/6 pole, 12 kW test model operating at 220 V at 6000 rpm with a peak current limit of 210 A.

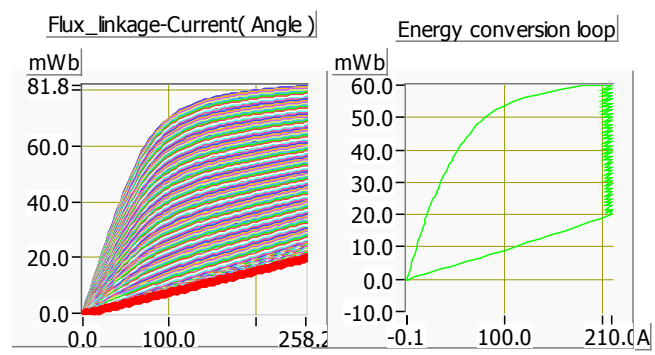

Fig. 5
Flux linkage-current curves and energy conversion loop for the 8/6 pole, 12 kW SRM at rated conditions and current control.

Fig. 6 shows the waveforms of applied voltage, phase current and torque, flux linkage and corresponding inductance for a single stator pole at rated conditions. Taking the fully unaligned position as angular reference, the controller turns the voltage on at the 7.5 deg position and turns it off at the 22.5 deg position so that the dwell angle is 15 deg. The resulting mean current and torque are 46.0 A and 23.2 N-m respectively. These calculated values compare well with the measured values.

Fig. 7 shows the flux lines of the same 8/6 pole, 12 kW SRM motor computed using the finite element magnetics (FEM) code FLUX-2D. The position shown in Fig. 7 corresponds to the instant prior to voltage reversal to avoid breaking torque. The calculated peak air gap flux density with this code was 2.0 Tesla.

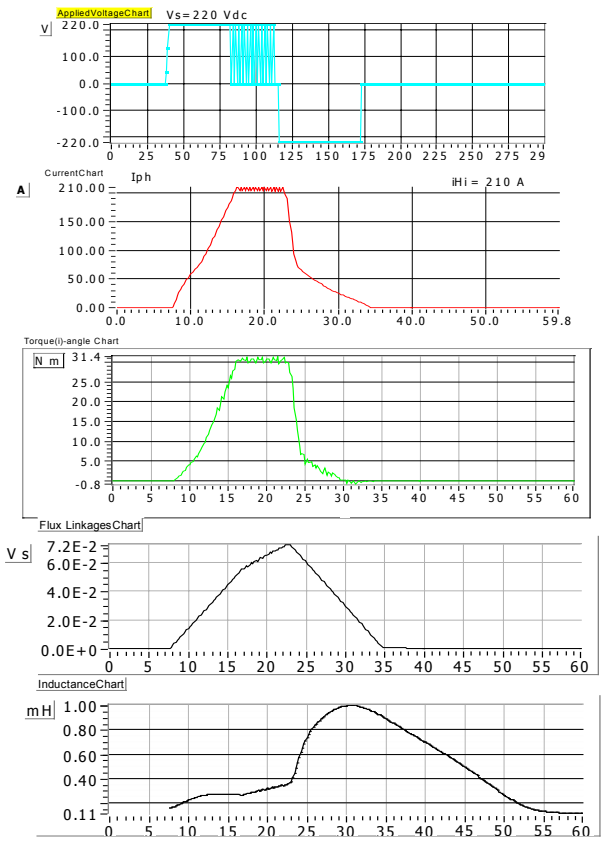

Fig. 6.
Waveforms of input voltage, phase current and torque lines of the 8/6 pole, 12 kW SRM as a function of rotor position

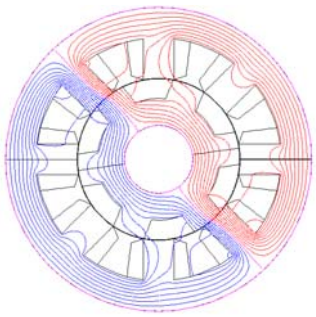

Fig. 7
FEM computed flux lines of the 8/6 pole, 12 kW SRM.

III. Analysis of Test Models

To validate the models, values measured in house and values provided by the vendors of an 8/6 pole, 12 kW SRM and a 24/16 pole, 35 kW SRM were compared with values calculated by the program.

A.- The 8/6 Pole, 12 kW SRM

The 8/6 pole, 12 kW SRM, produces a torque of 20 N-m at 6000 rpm driven by a 4-phase 220 V source. Essential to validation is the comparison of the relationships of flux linkages and torque to the value of the stator's current.
Flux linkages versus current curves were obtained by integration of the transient voltage and current waveforms as the stator winding was loaded with current with the rotor locked at a number of positions between the fully unaligned and fully aligned. Fig. 8 shows the computed and measured flux linkages as a function of phase current at the fully aligned position.

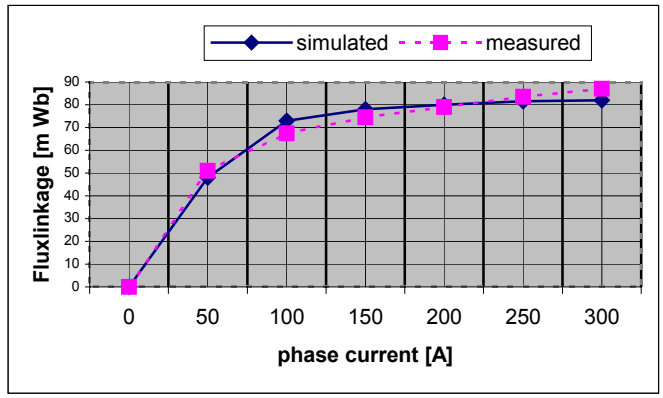

Fig. 8
Flux linkage vs. phase current of the 8/6 pole, 12 kW SRM in fully aligned position.

The torque map calculated with Eq. 13, as a function of rotor position for currents in steps of 10 A, is shown in Fig. 9. The computation starts at the fully unaligned rotor position (0 deg) and ends at the fully aligned position (30 deg).

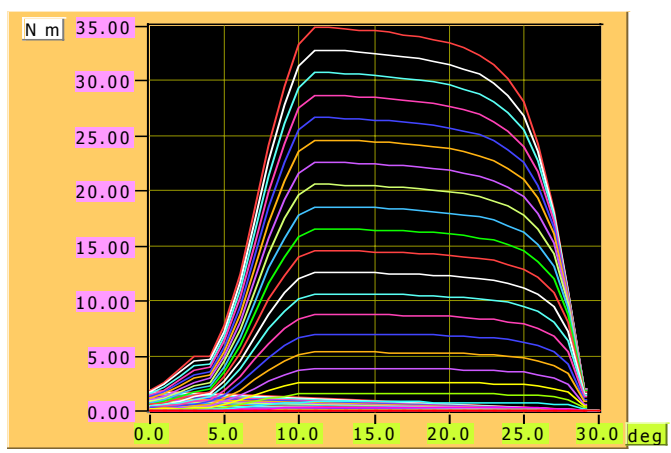

Fig. 9
Map of Torque-Current for the 8/6 pole, 12 kW SRM as function of rotor position

Fig. 10 shows the torque-current curves as function of rotor position for a phase current limit of 210A, μ_r of 3500, and B_{sat} of 2.05 Tesla. For comparison the values obtained with the FEM program and measured are also included. In all three curves the maximum torque occurred at the same 12 degree

position. The two computed peak values are similar but slightly higher than the measured. It was been found later that a range measuring error was made with the torque meter used.

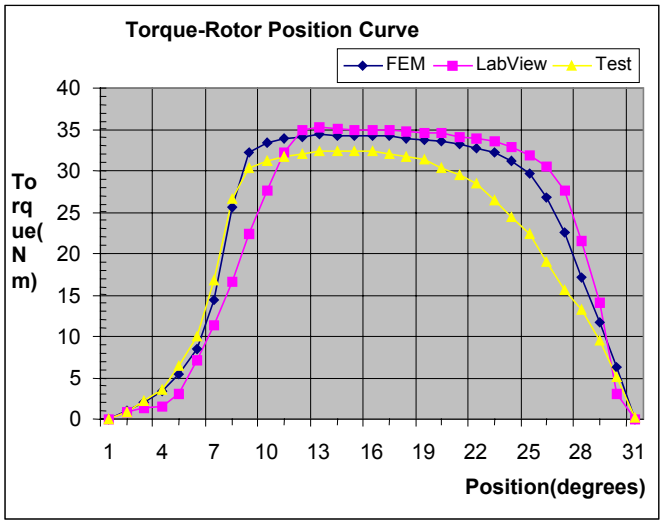

Fig. 10
Comparisons of torque vs. rotor position for the 8/6 pole, 12 kW SRM simulation with a 210 A current limit.

A comparison of the experimental and simulated torque vs. current curves is shown in Fig. 11. The differences observed are attributable to differences in the firing and turn-on angles used.

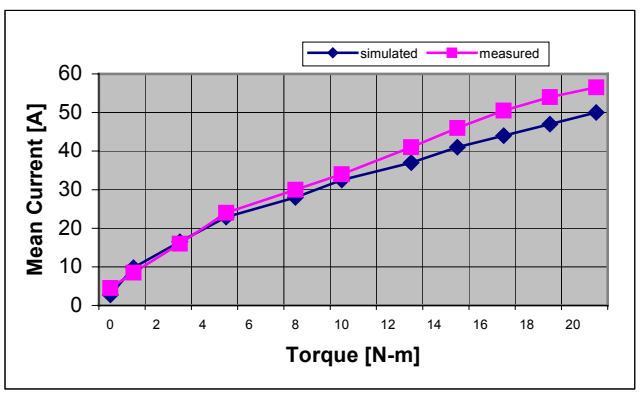

Fig. 11
Comparisons of mean torque vs. mean Current for the 8/6 pole, 12 kW SRM with a 210 A current limit.

B. The 24/16 pole 35 kW SRM

The 24/16 pole, 35 kW SRM has a dual axle configuration where each module produces a torque of 334 N-m at 500 rpm (i.e., 17.5 kW) and it is driven by a 3-phase 220 V source. The schematic of the FEM simulation is shown in Fig.12 with the rotor shown in fully unaligned position and one phase coil energized.

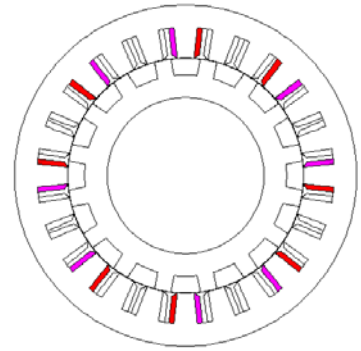

Fig. 12
Schematic of 24/16 pole, 35 kW FEM SRM simulation

Fig.13 shows the computed waveforms of applied voltage and phase current at 300 V, 150 A, and 300 rpm in the simulation. The simulated results agree with the measured values within 3 %.

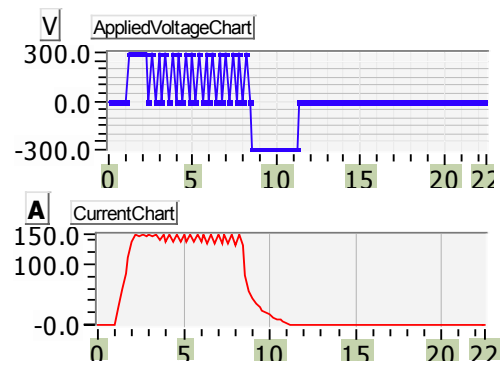

Fig. 13
Voltage and current waveforms at 300V, 150 A, 300 rpm of 24/16 pole 35 kW SRM model with current control.

Fig.14 shows the motor's output power as a function of speed under the nominal operation conditions of V_s = 300 V, limit current of 170 A for 3 different power turn-on angles and the same turn off angle. The output power (or torque) depends on the voltage turn on and dwell angles. As the dwell angle increases the maximum power increases up to the point at which breaking torque is produced.

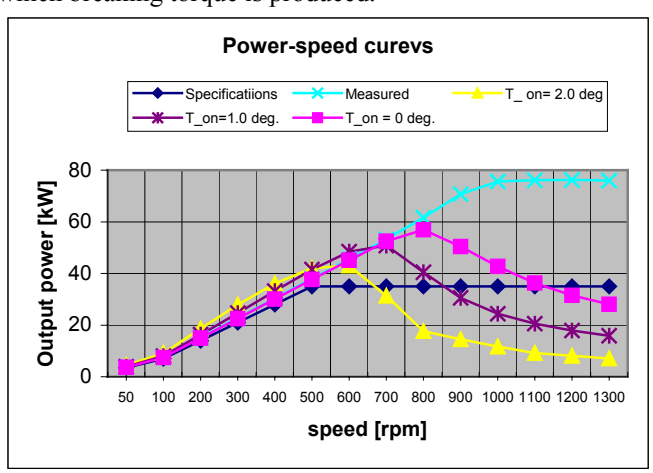

Fig. 14.
Comparison of output power vs. speed curves for the 24/16 pole 35 kW SRM at 0, 1, and 2 deg turn-on angles

In figures 15a and 15b, the simulated results of torque and output power are compared with the specified and the measured values under continuous operation conditions.

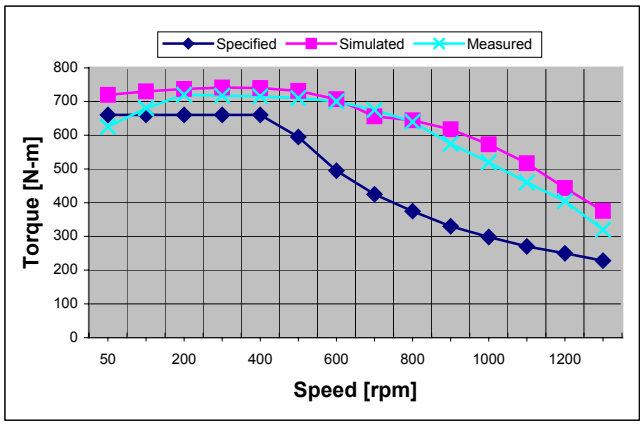

Fig. 15a
Comparison of the 24/16 pole 35 kW SRM's torque as a function of speed at 300 V and 170 A peak current limit.

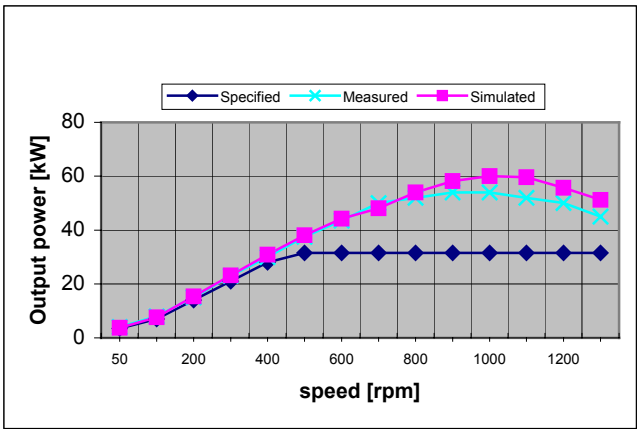

Fig. 15b
Comparison of the 24/16 pole 35 kW SRM's power as a function of speed at 300 V and 170 A peak current limit.

Up to the base speed the dwell angle was constant at 7.9 degrees. At higher speeds the dwell angle was increased up to 10.4 degrees. The calculated results compare well with the measured values.

Fig.16 compares calculated and measured efficiency curves for the base values of 300 V, and peak current limit of 170 A. The simulated and measured values compare well in the whole range of speeds.

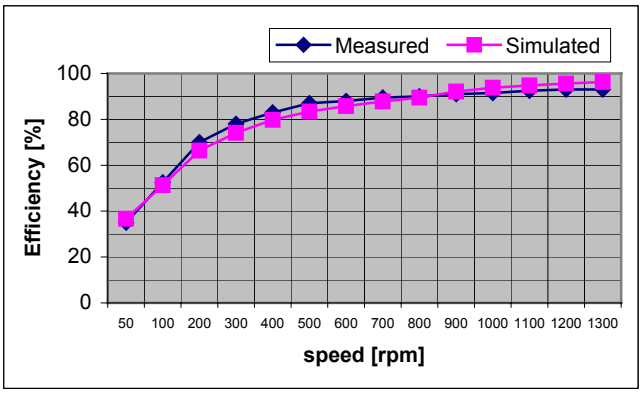

Fig. 16
Efficiency of the 24/16 pole, 35 kW SRM as a function of speed for 300 V and peak current limit of 170 A.

Fig. 17 shows a comparison of the simulation results for torque as a function of rotor position. In the results of the FEM calculation, the torque shows a sharp knee when the poles start to overlap. This is attributed to the dependence of the torque on the saturation flux density, B_{sat}, and the interpolation algorithm used in the CAD program (written in LabVIEW) to smooth the unaligned-to-aligned transition region. Beyond the 6 degree position, the two computational approaches produce values in reasonably good agreement.

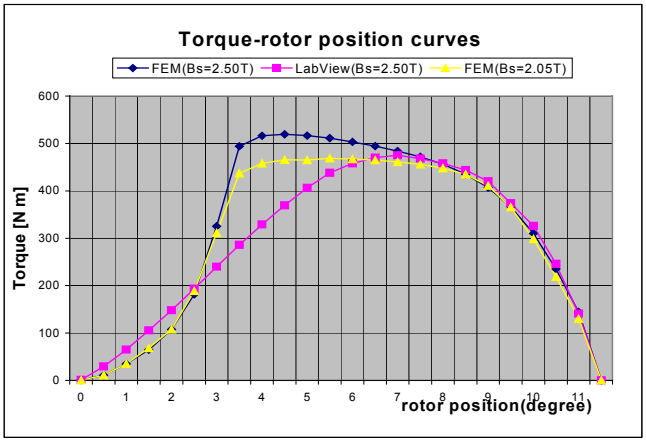

Fig. 17
Torque vs. current of the 24/16 pole, 35 kW SRM as a function of rotor position.

IV. Conclusion

In this paper, an interactive design and analysis program has been described for switched reluctance motors using an analytical method and a CAD program written in *LabVIEW*. The method uses conventional permeance algorithms, in which flux linkages, inductances and torques are calculated numerically. The performance data from detailed single pole flux-linkage analysis for the source voltage, current control, and firing and turn-off angles are cloned to generate waveforms for the remaining poles and phases to obtain mean values for each full turn of the rotor.

Two motors, an 8/6 pole, 4 phase, 12 kW and an 24/16 pole, 3 phase, 35 kW were analyzed under the given specifications and constraints and results compared with measured data.
The study has shown that by controlling the current limit, voltage and turn-on and dwell angles, constant output power can be obtained in these two SRMs even in the high-speed region.

ACKNOWLEDGMENTS: This work was supported by the DOE Office of Transportation Technologies and the Korean Research Foundation (KRF-2000-EA0044).

V. REFERENCES

[1] T. J. E. Miller, '*Switched Reluctance Motors and their Control*', MagnaPhysics Publishing and Clarendon Press, Oxford, 1993.
[2] D. C. Hanselman, '*Brushless Permanent-Magnet Motor Design*', McGraw-Hill, Inc., 1994.
[3] P. Lawrenson et al., Variable-speed switched reluctance motors, IEEE Proceedings Vol.127, Part B, No. 4, pp. 253-265, July 1980.
[4] A. V. Radun, "Design Consideration for the Switched Reluctance Motor", IEEE Transactions on IA, Vol. 31, No. 5, pp.1079-1087, September/October 1995.
[5] A. V. Radun, "Analytically Calculating the SRM's Unaligned Inductances", IEEE Transactions on Magnetics, Vol. 35, No. 6, pp.4474-4481, November/December 1999.
[6] A. V. Radun, "Analytically Computing the Flux Linked by a Switched Reluctance Motor Phase When the Stator and Rotor Poles Overlap", IEEE Transactions on Magnetics, Vol. 36, No. 4 pp.1996-2003, July 2000.
[7] P. Shin, P. Otaduy and J. McKeever, 'Design and Simulation Program for Switched Reluctance Motor', ORNL-2001/132, July 2001.
[8] R. Davis, W. Ray and R. Blake, Inverter drive for switched reluctance motor: circuits and component ratings, IEEE Proceedings Vol. 128, Pt. B, No. 2, pp. 126-136, March 1981.
[9] I. Boldea and S. A. Nasar, '*Electric Drives*', CRS press, 1998.